Friction **10**(1): 142–158 (2022)
https://doi.org/10.1007/s40544-020-0471-3
ISSN 2223-7690
CN 10-1237/TH
RESEARCH ARTICLE

Robust low friction performance of graphene sheets embedded carbon films coated orthodontic stainless steel archwires

Zonglin PAN, Qinzhao ZHOU, Pengfei WANG*, Dongfeng DIAO

Institute of Nanosurface Science and Engineering (INSE), Guangdong Provincial Key Laboratory of Micro/Nano Optomechatronics Engineering, Shenzhen University, Shenzhen 518060, China

Received: 29 April 2020 / Revised: 21 September 2020 / Accepted: 04 November 2020

Abstract: Reducing the friction force between the commercial archwire and bracket during the orthodontic treatment in general dental practice has attracted worldwide interest. An investigation on the friction and wear behaviors of the uncoated and carbon film coated stainless steel archwires running against stainless steel brackets was systematically conducted. The carbon films were prepared at substrate bias voltages from +5 to +50 V using an electron cyclotron resonance plasma sputtering system. With increasing substrate bias voltage, local microstructures of the carbon films evolved from amorphous carbon to graphene nanocrystallites. Both static and stable friction coefficients of the archwire-bracket contacts sliding in dry and wet (artificial saliva) conditions decreased with the deposition of carbon films on the archwires. Low friction coefficient of 0.12 was achieved in artificial saliva environment for the graphene sheets embedded carbon (GSEC) film coated archwire. Deterioration of the friction behavior of the GSEC film coated archwire occurred after immersion of the archwire in artificial saliva solution for different periods before friction test. However, moderate friction coefficient of less than 0.30 sustained after 30 days immersion periods. The low friction mechanism is clarified to be the formation of salivary adsorbed layer and graphene sheets containing tribofilm on the contact interfaces. The robust low friction and low wear performances of the GSEC film coated archwires make them good candidates for clinical orthodontic treatment applications.

Keywords: graphene sheets; carbon film; archwire; low friction; artificial saliva

1 Introduction

Orthodontic treatment is the restoration of the abnormally positioned teeth for human beings, especially for children and teenagers with dramatically increasing oral health and beauty requirements in recent years [1–5]. The fixed orthodontic appliance consisting of archwire and bracket has been extensively applied for dental clinical applications. The relative sliding of the archwire to bracket produces first static and then kinetic friction forces, which greatly affects the tooth movement efficiency [6–9]. The achievement of low friction forces could strongly reduce the risk of root resorption and patient pain, shorten the treatment time, and improve both anchorage control and direction of tooth movement. Therefore, reducing the friction force (no matter static or kinetic) between the orthodontic archwire and bracket has drawn worldwide interest not only from clinicians in clinical stomatology fields but also scientists in surface engineering fields [10–12].

Numerous attempts have been carried out in the last two decades for minimizing the friction resistances between archwires and brackets. Particularly, surface coating technique is clarified as one of the most effective strategies for tailoring the friction and wear behaviors of the archwire-bracket contact systems

* Corresponding author: Pengfei WANG, E-mail: wangpf@szu.edu.cn

[13–18]. Katz et al. found that the inorganic fullerene-like WS_2 nanoparticles embedding self-lubricating nickel-phosphorous film reduce the friction coefficient to 0.05 for the coated stainless steel archwire [13]. Akaike et al. reported that the fluorine-doped diamond-like carbon film coated archwire demonstrates lower static friction force than the uncoated archwire in both dry and wet conditions [14]. Wei et al. clarified that the carbon nitride thin film significantly reduces the friction force of the archwire-bracket sliding contacts in ambient air and artificial saliva environments [15].

Since the discovery of graphene in 2004, the graphene and derived products have emerged as star-materials for advanced and cutting-edge applications [19]. On the one hand, the superior antibacterial, biocompatible, inexpensive, and sustainably available characteristics of the graphene-based materials make them suitable for demanding biomedical and clinical applications [20–23]. On the other hand, superlubricity (friction coefficient in the order of 0.01 or less) of the single layer or few layers graphene enables the possible design of frictionless sliding contacts in practical engineering applications [24–27]. In the previous researches of our group, the embedding of graphene nanocrystallites into amorphous carbon matrix promotes the formation of graphene sheets embedded carbon (GSEC) films with highly active graphene edge defects, which presenting unique mechanical (surface roughness less than 0.1 nm), magnetic (12% of magnetoresistance at room temperature), electrochemical (potential window larger than 3.2 V), and even optoelectronic (photocurrent responsivity of 0.35 A/W) properties [28–30]. Therefore, the purpose of this research is to optimize the friction and wear performances of the archwire-bracket sliding contacts by depositing GSEC films on the commercial stainless steel archwires with an electron cyclotron resonance (ECR) plasma sputtering system. Low friction coefficients and high wear resistance of the stainless steel archwire-bracket tribo-couples were achieved in artificial saliva environment through the fabrication of GSEC films on the archwires. The low friction mechanism of the GSEC film coated archwires was discussed in terms of structural changes on the contact interfaces.

2 Experimental details

2.1 Materials

Commercially obtained orthodontic stainless steel archwire (HXH-0023, Xihubiom, Xihu Biomaterials Co., Ltd., Hangzhou, China) with a cut length of 110 mm and cross-sectional dimensions of 0.017 inch (0.42 mm) × 0.025 inch (0.64 mm) was employed in this work. The archwire was fitted in a stainless steel bracket (torque and/or angulation of 0°) with a slot of 0.22 inch (0.56 mm) (ALS-0008, Alice Dental Medical Equipment Co., Ltd., Hangzhou, China). The combined archwire and bracket was utilized only once to avoid the potential effects from the strain of archwire and the abrasion of bracket. Prior to film deposition and friction test, all archwires and brackets were consecutively cleaned with acetone, ethanol, and deionized water by an ultrasonic cleaner (M2800-C, Branson, China). Each solution was used separately for 20 min to clean organic compounds and inorganic substances at the surfaces of archwires and brackets.

Treated archwires were fixed in a vacuum chamber of a mirror confinement electron cyclotron resonance (MCECR) plasma sputtering system by a custom designed jig, and the background pressure was 8×10^{-5} Pa. Detailed information about the self-developed deposition system could be found in Refs. [31–33]. After purging argon (Ar) gas to achieve a pressure of 0.1 Pa, the surfaces of archwires were firstly etched by an Ar plasma for 3 min with a substrate bias voltage of –50 V, and then carbon films were deposited onto the sliding contact surfaces (width of 0.017 inch) of the archwires with substrate bias voltages under +5, +10, +20, and +50 V. Low energy electron irradiation is realized by using a positive substrate bias voltage [33–35]. The deposition time was set at 30 min, and the thickness of the film was approximately 100 nm. Specific deposition parameters are summarized in Table 1.

2.2 Film characterization

Surface morphology and elemental composition of the uncoated and carbon film coated archwires were examined by using a scanning electron microscope (SEM, Scios, FEI, USA) operated at an electron

Table 1 Conditions of carbon films deposition.

Deposition parameter	Value
Base pressure (Pa)	8×10^{-5}
Deposition pressure (Pa)	0.1
Ar gas flow ratio (sccm)	12.8
Microwave power (W)	500
Target bias voltage (V)	–500
Substrate bias voltage (V)	+5, +10, +20, +50

acceleration voltage of 10 kV in association with an energy dispersive X-ray spectroscope (EDS).

A three-dimensional laser confocal microscope (VK-X250K, Keyence, Japan) was used to evaluate the surface roughness of the carbon film coated archwires and analyze the wear scars on the worn surfaces of the carbon film coated archwires. The surface roughness was measured three times and an average value was applied.

The bonding structure configurations of the carbon films were obtained using a Raman spectroscope (LabRAM HR Evolution, Horiba, Japan) at a laser wave length of 532 nm and a spectrum region between 800 and 3,500 cm^{-1}.

The nanostructures of the as-deposited carbon films were investigated with a double spherical aberration corrected high-resolution transmission electron microscope (HRTEM, Titan 3 Themis G2, FEI, USA) and an electron energy loss spectroscope (EELS, GIF Quantum ER/965 P, Gatan, USA). An electron acceleration voltage of 80 kV was applied to avoid potential damages from high energy electron irradiation.

2.3 Friction tests

Friction and wear behaviors of the archwire-bracket combination were systematically evaluated with a home-built reciprocating sliding tribometer, as shown in Fig. 1. The customized tribometer consists of two parts, as shown in Fig. 1(a), one is the reciprocating sliding friction system, including a bracket holder, an archwire holder, a cantilever beam, a stepper motor, a three-axis stage, and a waste liquid collecting tank. The other is the artificial saliva supply system, containing a beaker, a peristaltic pump, a thermostat water bath, a tube as well as a magnetic stand. Commercially available artificial saliva was supplied to the contact interface of the archwire and bracket with the adjustments of dripping speed and temperature by using a peristaltic pump and a thermostat water bath, respectively. The used artificial saliva was gathered in a waste liquid collecting tank. A bracket was firstly stuck on the surface of an aluminum block by glue, and then was fixed in the bracket holder, as shown in Fig. 1(b). The bracket holder was installed at one end of the cantilever beam which was attached

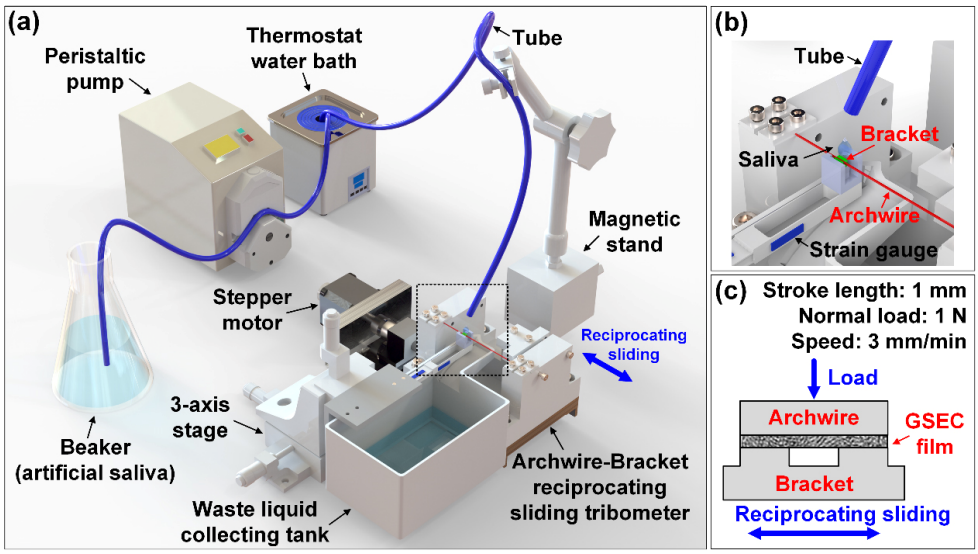

Fig. 1 Experimental configurations for a home-built reciprocating sliding tribometer for evaluating friction and wear behaviors of the orthodontic archwire-bracket combination. (a) 3D structural diagram; (b) enlarged view of the contact combination of the archwire and bracket; and (c) sliding contact model of the GSEC film coated archwire and bracket.

to a stationary three-axis stage. Thereafter, an archwire was fixed in the archwire holder and pre-stretched with a tensile force of around 10 N. The archwire holder was mounted on a stepper motor (TSA50-C, Zolix, China) for controlling the relative sliding between the archwire and bracket. The archwire was moved to pass through the slot of the bracket. The sliding contact model of the carbon film coated archwire and slot surface of the bracket with no ligation is shown in Fig. 1(c). Two sets of strain gauges (horizontal and vertical directions) were cemented on the cantilever beam for detecting the friction force and normal force during the movement of the archwire and bracket. The data of the friction force and normal force was simultaneously recorded by a computer.

The reciprocating sliding friction tests were performed at a stroke length of 1 mm under a sliding speed of 3 mm/min as well as a normal force of 1 N. The number of reciprocating movements was set to be 100 times (around 4,000 s) according to the number of contacts for a single archwire in the orthodontic treatment [36]. Friction tests were conducted in both dry (ambient air, room temperature of 25 °C and relative humidity of 60 %RH) and wet (artificial saliva) conditions. Commercially available artificial saliva (pH=6.9) containing mainly 0.4 g/L NaCl, 0.4 g/L KCl, 0.795 g/L $CaCl_2$, 0.78 g/L NaH_2PO_4, 0.005 g/L Na_2S, and 1 g/L urea was employed in this study. The temperature of the artificial saliva was maintained at 37 ± 0.5 °C to simulate the human oral environment with a thermostat water bath (BHS-1, Joanlab, China). The artificial saliva was supplied to the contact interface of the archwire and bracket with a tube (inner diameter of 3.2 mm) under a dripping speed of 3.6 mL/min by using a peristaltic pump (BT100J-1A, Huiyu, China). After friction tests, the worn archwires were thoroughly cleaned in an ultrasonic cleaner with deionized water for 5 min to eliminate the artificial saliva on the archwires. The surface conditions of archwires before and after friction tests were analyzed by an optical microscope (LV150N, Nikon, Japan) and a 3D laser confocal microscope.

2.4 Immersion test

To assess the corrosion resistance of the carbon film coated archwires, the specimens were immersed in the artificial saliva solution. The carbon film coated archwires were placed in the artificial saliva solution with the side of the carbon film facing up. According to the replacement cycle of a single archwire in the clinical orthodontic treatment [36, 37], the archwire was observed and investigated with a time interval of 0, 10, 20, and 30 days. Before and after the immersion test, worn surfaces of the archwires were observed with an optical microscope and a 3D laser confocal microscope.

3 Results and discussion

3.1 Composition and structural analysis of carbon films

In the present work, carbon films were fabricated on the surfaces of stainless steel archwires by using an MCECR plasma sputtering system. The surface roughness of the uncoated and carbon film coated archwires deposited at various substrate bias voltages is given in Table 2. The surface roughness of the as-received stainless steel archwire is 0.031 μm. The surface roughness of the archwire increases with the production of the carbon film. Specifically, the surface roughness of the carbon film coated archwire increased gradually from 0.043 to 0.053 μm with the increase of substrate bias voltage from +5 to +50 V.

SEM images of the as-received stainless steel bracket and stainless steel archwire were shown in Figs. 2(a)–2(d). A relative smooth surface was observed on slot surface in the bracket. SEM image of a typical carbon film coated stainless steel archwire was shown in Fig. 2(d). It can be found in Figs. 2(c) and 2(d) that micro-grooves generated in the production process of the stainless steel archwire were clearly observed even after the deposition of the carbon film under the substrate bias voltage of +50 V. Besides, small particles were randomly distributed on the surface of the carbon film coated archwire.

Table 2 Surface roughness of the uncoated and carbon film coated stainless steel archwires fabricated at different substrate bias voltages.

Film condition	Uncoated	+5 V	+10 V	+20 V	+50 V
Ra (μm)	0.031	0.043	0.046	0.051	0.053

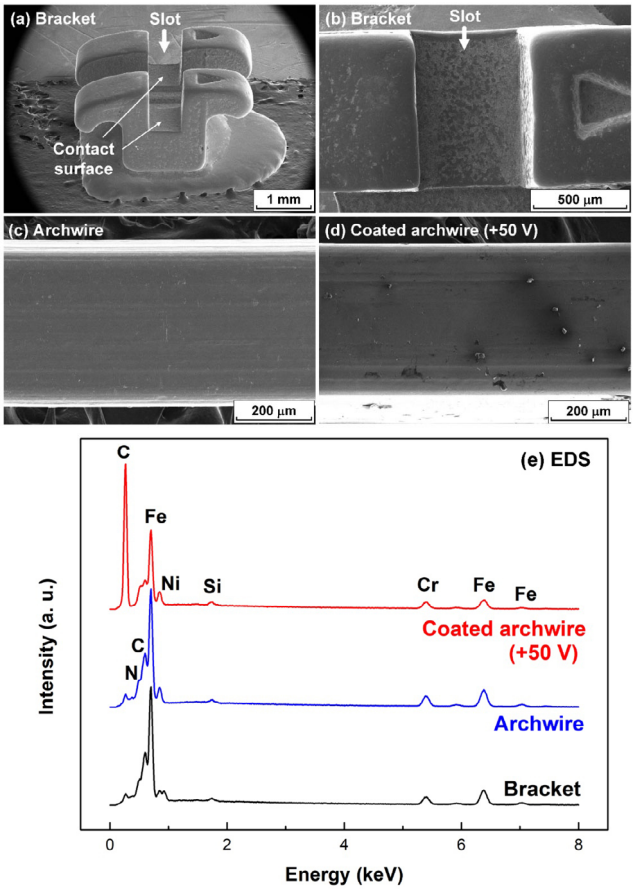

Fig. 2 SEM images of (a) a conventional stainless steel bracket, (b) an enlarged view of slot surface of stainless steel bracket, (c) an as-received stainless steel archwire, and (d) a carbon film coated stainless steel archwire (substrate bias voltage of +50 V). (e) EDS spectra of a stainless steel bracket, an uncoated stainless steel archwire, as well as a carbon film coated archwire (substrate bias voltage of +50 V).

Representative EDS spectra of the uncoated and carbon film coated archwire and bracket were shown in Fig. 2(e). Typical peaks of N, C, Fe, Ni, Si, and Cr could be seen in the spectra of stainless steel archwire [15, 38] and bracket. Strong peak of C with a lower energy in the spectrum of carbon film coated archwire was mainly ascribed to the growth of the carbon film.

Raman spectra of the carbon films prepared at various substrate bias voltages were shown in Fig. 3. The Raman spectrum of the carbon film generally contains a D peak (sp^2 bonding state of carbon atoms in clusters of sixfold aromatic rings) and a G peak (sp^2 bonding state of carbon atoms in rings and chains) at approximately 1,350 and 1,600 cm^{-1}, respectively. The shapes of the D and G peaks become sharper and more distinct with increasing substrate bias voltage from +5 to +50 V. Besides, a compound 2D peak (typical feature in graphene or graphite samples) centered around 2,800 cm^{-1} was observed on the Raman spectra of the carbon films produced at substrate bias voltages of +5 and +10 V, as shown in Figs. 3(a) and 3(b). However, two separate 2D peaks were detected on the Raman spectra of the carbon films produced at substrate bias voltages of +20 V and +50 V, as shown in Figs. 3(c) and 3(d). According to the previous researches [39, 40], the change of the 2D peak shape in the carbon films strongly implies a phase transition from amorphous carbon structure to an ordered graphene nanocrystalline structure with the increase of substrate bias voltage from +5 to +50 V.

The prominent D peak and G peak of the Raman spectrum ranging from 1,100 to 2,000 cm^{-1} were fitted with a Lorentzian peak and a Breit-Fano-Wagner (BFW) peak, respectively [41−43], after a background subtraction, as shown in Figs. 3(e)−3(h). The D peak shifts to a lower frequency with the increase of the substrate bias voltage and varies slightly among 1,341 and 1,345 cm^{-1}. Additionally, the height ratio of the D peak intensity to G peak intensity (denoted as I_D/I_G thereafter) increases substantially from 0.65 to 0.95 with increasing substrate bias voltage from +5 to +50 V, as listed in Table 3. The in-plane size (L_α) of graphene nanocrystallites in the carbon films was calculated based on the above-mentioned I_D/I_G values by using the equation of $I_D/I_G = C(\lambda)\ L_\alpha^2$, where $C(\lambda)$ is equal to 0.55 nm^{-2} [32, 34], the corresponding results are shown in Table 3. The size of the graphene nanocrystallites increases gradually from 1.09 to 1.31 nm with the increase of substrate bias voltage from +5 to +50 V. Therefore, it is concluded that higher substrate bias voltage results in stronger graphene nanocrystallization of the prepared carbon films on the stainless steel archwire.

The nanostructure information of the carbon films on the surfaces of the stainless steel archwires was further characterized by a high-resolution TEM, as shown in Fig. 4. Figs. 4(a) and 4(b) show the plan view TEM images of the carbon films fabricated at the substrate bias voltages of +5 and +50 V, respectively. The inset fast Fourier transformation (FFT) image of

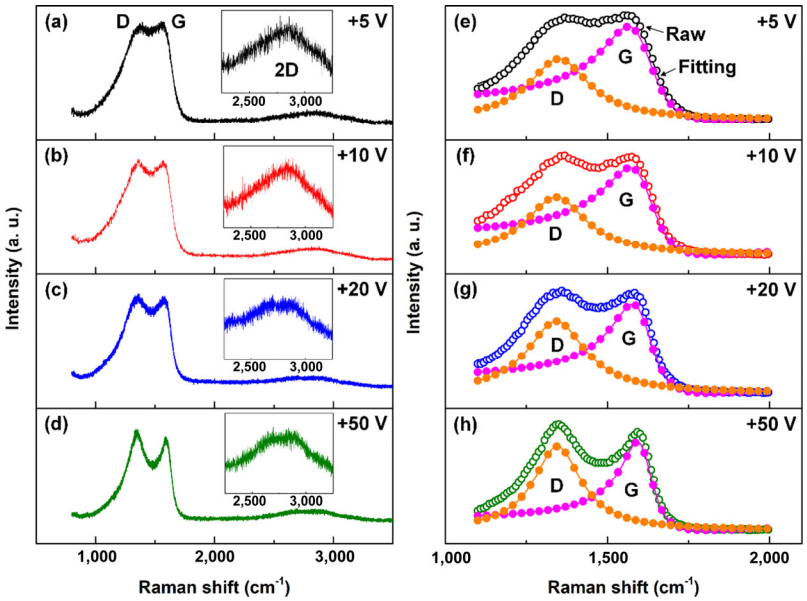

Fig. 3 Raman spectra and corresponding deconvolution curves (a Lorentzian peak for the D band and a BFW peak for the G band) of the carbon films prepared at substrate bias voltages of (a, e) +5 V, (b, f) +10 V, (c, g) +20 V, and (d, h) +50 V. Enlarged views of the 2D peak(s) are shown in the inset images.

Table 3 Raman analysis results of the carbon films deposited at different substrate bias voltages.

Substrate bias voltage (V)	D peak (cm^{-1})	I_D/I_G	L_α (nm)
+5	1,350	0.65	1.09
+10	1,341	0.66	1.10
+20	1,342	0.81	1.21
+50	1,345	0.95	1.31

the selected white color square region (no special pattern or white light spot in Fig. 4(a)) demonstrated an amorphous structure in the carbon film prepared under substrates bias voltage of +5 V. FFT image of the selected yellow color square region (two white light spots in Fig. 4(b)) indicates the existence of multilayer graphene sheets (an average interlayer spacing of 0.34 nm) in the carbon film prepared under substrates bias voltage of +50 V. Graphene nanocrystallites (marked with yellow dotted circles) with a maximum layer number of less than five are uniformly distributed in the carbon films, as indicated in Fig. 4(b). Graphene edges are easily observed at the borders of the graphene nanocrystallites.

EELS spectra in the C-*K* edge region were employed to further elucidate the nanostructures of the carbon films. Figures 4(c) and 4(d) show the *C-K* edge core-loss

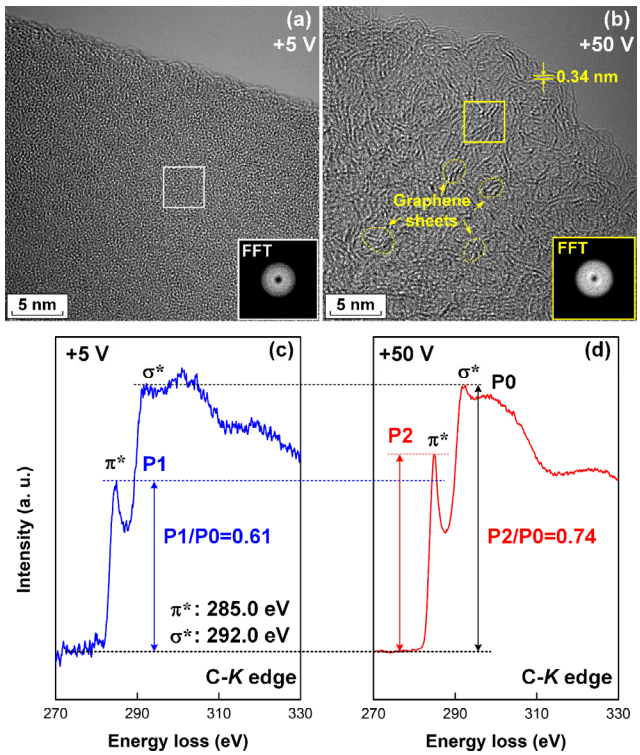

Fig. 4 Nanostructures of the carbon films observed by HRTEM. (a) The plan view TEM image and (c) C-*K* edge core-loss EELS spectrum for the carbon film prepared at the substrate bias voltages of +5 V. (b) The plan view TEM image and (d) C-*K* edge core-loss EELS spectrum for the carbon film prepared at the substrate bias voltages of +50 V. Inset figures in (a) and (b) indicate FFT images of the marked square regions in the corresponding TEM images.

spectra for the carbon films produced under the substrates bias voltages of +5 and +50 V, respectively. Two feature peaks locate around 285.0 and 292.0 eV, corresponding to π^* peak (sp^2 bonding carbon atom) and σ^* peak (crystalline structure in carbon film), respectively, are observed in the *C-K* edges after removal of the background signal. The intensity of the two peaks and the shape of the spectrum are highly related to the nanostructures of the carbon films [44–46]. The normalized height ratio of π^* peak to σ^* peak (denoted as $\pi*/\sigma*$ thereafter) increases from 0.61 to 0.74 with the increase of substrate bias voltage from +5 to +50 V. Therefore, it is suggested that higher sp^2/sp^3 ratio is obtained in the carbon film fabricated at a higher substrate bias voltage.

The TEM images and EELS spectra provided a direct evidence of the formation of multilayer graphene sheets in the carbon films. It is clearly demonstrated that higher energy of electron irradiation induces the growth of the graphene nanocrystallites. Therefore, it was further confirmed that higher energy of electron irradiation is beneficial for achieving an ordered graphene nanocrystallites layer structure in carbon films grown by an ECR plasma system [29, 34, 42]. The growth mechanism of the GSEC films has been attributed to the inelastic scattering of the electron in Ref. [40]. Besides, the formation of sp^2 clusters generally leads to surface roughening of the carbon films [47], resulting in an increase of the surface roughness of the carbon film coated archwire (shown in Table 2).

According to the abovementioned analysis results, it is unraveled that the local nanostructures of the carbon films evolve from an amorphous phase or small size sp^2 nanocrystallites domains in low substrate bias voltages (+5 and +10 V) to a highly ordered or multilayer graphene sheets embedded carbon matrix structures in relatively high substrate bias voltages (+20 and +50 V), as clearly revealed by the Raman and TEM-EELS characterizations.

3.2 Tribological behavior of the archwire-bracket system

Friction and wear behaviors of the archwire-bracket contact combinations were evaluated in both dry and wet conditions, as summarized in Fig. 5. Typical friction curves of the uncoated and GSEC film (substrate bias voltage of +20 V) coated archwires sliding against stainless steel brackets under wet conditions are shown in Figs. 5(a) and 5(b), respectively. Specifically, the friction coefficient increases sharply and reaches a stable value up to 0.50 for the uncoated stainless steel archwire sliding against bracket in wet conditions. However, when the carbon film coated archwire rubs against bracket in artificial saliva condition, friction coefficients less than 0.20 are observed from the initial stage and a steady state around 0.15 is established after 100 seconds. Friction curves of the uncoated and carbon film coated archwires sliding against brackets in dry condition are demonstrated in Figs. S1(a) and S1(b) in the Electronic Supplementary Material (ESM), respectively. Mean friction coefficients of four types of contact combinations in each cycle (totally 100 cycles) during sliding tests are calculated and are plotted in Fig. 5(c). Friction coefficients are higher than 0.50 that observed in the contact combinations including uncoated archwires, friction coefficients are lower than 0.20 that achieved for sliding contacts of the carbon film coated archwire no matter in dry or wet conditions. Typical friction curves in one cycle (i.e. two sliding strokes) at steady state from 3,000 to 3,040 s are drawn in Fig. 5(d). It can be found that carbon film coated archwires not only provide lower friction coefficients but also achieve smaller friction fluctuations compared with the uncoated archwires in both dry and wet conditions.

The maximum static friction coefficients and stable average friction coefficients of the uncoated and carbon film coated archwires sliding against brackets in dry and wet conditions are depicted in Fig. 5(e). The maximum static friction coefficient (μ_{stat}) is evaluated as the maximum value of the static friction coefficient of each cycle during the whole friction test. The stable average friction coefficient (μ_{stab}) is calculated as the average value of the friction coefficient during the final 1,000 seconds (from 3,000 to 4,000 s) of the sliding test. Representative friction curves for determining the maximum static friction coefficients of uncoated and carbon film coated archwires are shown in Figs. S2(a) and S2(b) in ESM, respectively.

It can be found that the carbon film facilitates the reduction of both the static friction coefficient and stable friction coefficient of the archwire-bracket contact

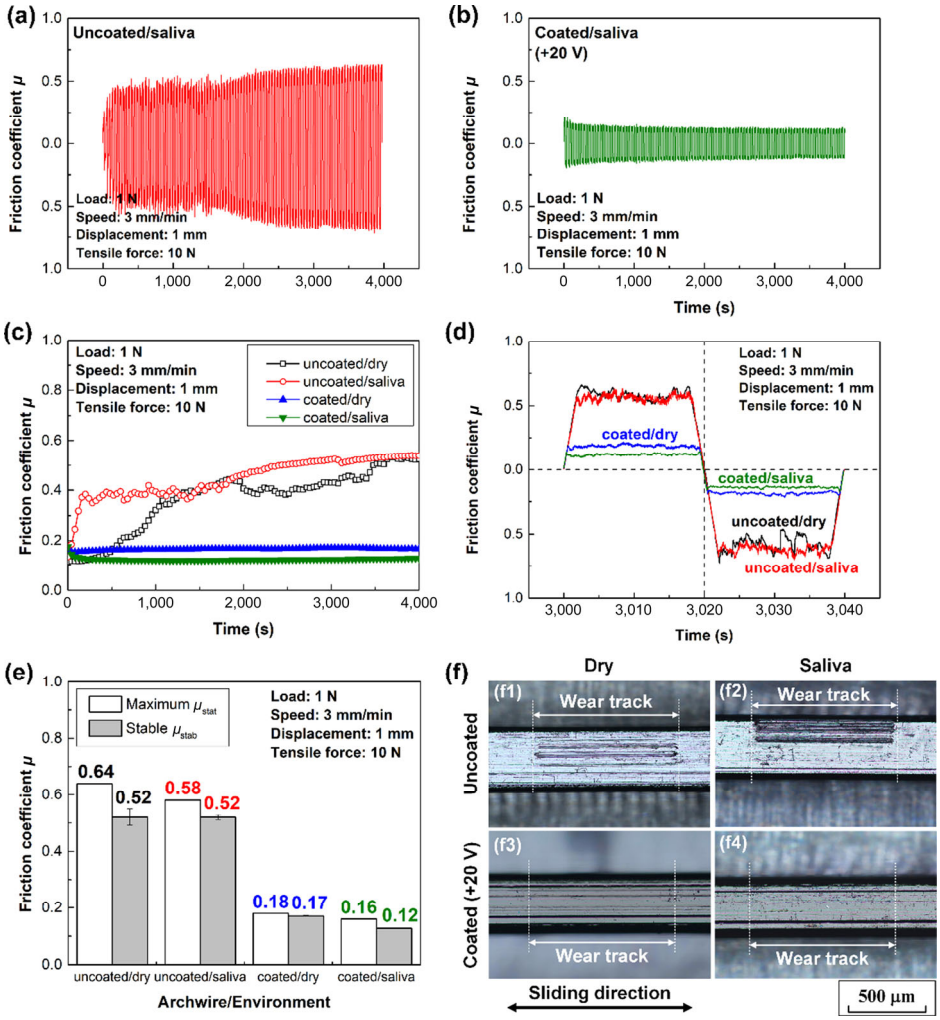

Fig. 5 Friction and wear behaviors of the contact combination of the archwires and brackets. (a) Typical friction curve of the uncoated archwire sliding against bracket under artificial saliva environment. (b) Typical friction curve of the carbon film (substrate bias voltage of +20 V) coated archwire running against bracket under artificial saliva environment. (c) Mean friction coefficients of each cycle for the uncoated and carbon film coated archwires rubbing against brackets under dry and wet conditions. (d) Typical friction curves in one cycle at steady state (3,000 to 3,040 s) of the uncoated and carbon film coated archwires sliding against brackets under dry and wet conditions. (e) Maximum static friction coefficients and stable average friction coefficients of the uncoated and carbon film coated archwires sliding against brackets in dry and wet conditions. (f) Optical images of worn surfaces on the uncoated and carbon film coated archwires after sliding against brackets in dry and wet conditions.

system. The uncoated archwire provides the highest static and stable friction coefficients of 0.64 and 0.52 in dry condition, while the carbon film coated archwire gives the lowest values of 0.16 and 0.12 in artificial saliva environment, respectively.

Optical images of worn surfaces on the uncoated and carbon film (substrate bias voltage of +20 V) coated archwires after sliding against brackets in dry and wet conditions are shown in Fig. 5(f). Optical images of the as-received stainless steel archwire and bracket are also given for comparison in Figs. S3(a) and S3(b) in ESM, respectively. Machining marks, such as grooves and pockmarks (Fig. S3(c) in ESM), because the manufacturing procedures (e.g. cutting and grinding) are clearly observed on the surfaces of the archwire and bracket, respectively. The wear tracks are clearly identified on the uncoated archwires, where micro-grooves due to the machining process are observed parallel to the sliding direction of the archwire-bracket contact. However, the wear tracks could barely be detected on the GSEC film coated archwires, the positions of the wear tracks are ascertained with the

assist of enlarged views of the images. It is therefore argued that friction and wear of the archwire is strongly determined by the deposition of the GSEC film other than the sliding environment. Adhesive and abrasive wear are the domain mechanisms for the uncoated archwires sliding with high friction coefficients in both dry and wet conditions. Mild wear occurred on the carbon film coated archwires with low friction coefficient in both dry and wet conditions.

Theoretically, the wear track should locate at the center of the archwire, as typically shown in Fig. 5(f1). The position of the wear track occasionally moves to the edge of the archwire, as shown in Fig. 5(f2), due to the misalignment of the archwire in relation to the bracket, which can hardly be eliminated in the archwire-bracket contact systems [48]. However, identical friction behaviors are achieved with the wear tracks locating at different regions of the archwires, as illustrated in Fig. S4 in ESM, the corresponding two friction tests are executed under the same experimental conditions. It has been confirmed that the friction behavior of the archwire shows less dependency on the location of the wear track in the present work.

With respect to the raw bracket, wear tracks on the brackets are concentrated at the external edge of the slot bottom surface, as definitely shown in Fig. S5 in ESM, which effectively mimick the wear mechanism of the bracket in the patient [48]. Severe scratches are observed on the worn surface, indicating abrasive wear of the bracket. Furthermore, the wear of the archwire and bracket seems unaffected by the experimental conditions.

3.3 Tribological behavior of carbon film coated archwire

To better understand the low friction behavior of the carbon film in artificial saliva environment, reciprocating sliding friction tests between brackets and carbon films coated archwires deposited at various substrates bias voltages were carried out in wet condition, the corresponding friction results are shown in Fig. 6. Mean friction coefficients of the four types of carbon film coated archwires sliding against brackets

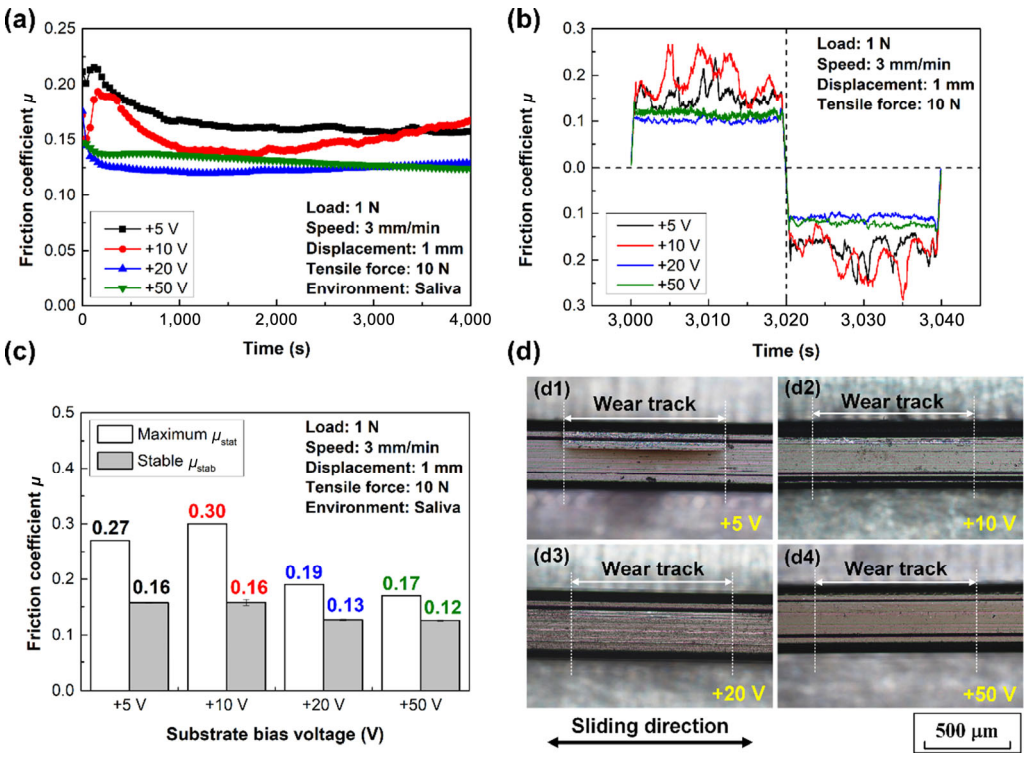

Fig. 6 Friction and wear behaviors of the carbon film coated archwires sliding against brackets under artificial saliva environment. The carbon films were produced on the surfaces of archwires at substrate bias voltages of +5, +10, +20, and +50 V. (a) Mean friction coefficients of each cycle. (b) Typical friction curves in one cycle at steady state from 3,000 to 3,040 s. (c) Maximum static friction coefficients and stable average friction coefficients. (d) Optical images of worn surfaces on the carbon film coated archwires.

under wet condition are given in Fig. 6(a). Low friction coefficients less than 0.25 are observed in all the carbon film coated archwires. In case of the amorphous carbon film (substrate bias voltages of +5 and +10 V) coated archwires, the friction coefficients first increase and then gradually decrease to a steady state. On the other hand, the friction coefficients of the GSEC film (substrate bias voltages of +20 and +50 V) coated archwires decrease from the beginning of the sliding test and quickly approach a steady state after 200 seconds. Friction fluctuations of different carbon films at steady state are added in Fig. 6(b). Lower friction fluctuation is obtained with the production of the GSEC films on the archwires. The maximum static friction coefficients and stable average friction coefficients of the carbon film coated archwires sliding against brackets in wet condition are shown in Fig. 6(c). Both the static and stable friction coefficients of the carbon film coated archwires decrease with the increase of the substrate bias voltage, with the lowest values of 0.17 and 0.12 are obtained at +50 V, respectively. It is thus argued that the GSEC film coated archwire is favorable for achieving low friction coefficients of the archwire-bracket tribo-systems in artificial saliva environment.

Optical images of worn surfaces on the carbon film coated archwires after sliding against brackets in wet condition are given in Fig. 6(d). Magnified views of the specific worn areas on the carbon film coated archwires are shown in Fig. S6 in ESM, clearly, delamination of the film as well as large amount of tribofilm is observed on the wear track of the carbon film coated archwire with carbon film deposited at substrate bias voltage of +5 V. The wear of the carbon film decreases with the increase of the substrate bias voltage. Particularly, mild wear occurs on the carbon film coated archwire at the substrate bias voltage of +50 V. As illustrated in Fig. S7 in ESM, morphological aspects of wear tracks on the slot bottom surfaces of brackets are identical with those observed in Fig. S6 in ESM, indicating mild wear of the brackets.

3.4 Immersion test of carbon film coated archwire

In order to assess the feasibility of the GSEC film coated archwires in clinical orthodontic treatment, immersion tests of the GSEC film (substrate bias voltage of +20 V) coated archwire were carried out in artificial saliva solution, the subsequent friction results are shown in Fig. 7. Mean friction coefficients of the GSEC film coated archwires sliding against brackets under artificial saliva environment after different immersion periods are given in Fig. 7(a). Generally, friction coefficients of the GSEC film coated archwires increase with the immersion periods. Slightly higher friction fluctuations of the GSEC film coated archwires at steady state are obtained with the increase of the immersion periods, as shown in Fig. 7(b). Furthermore, the maximum static friction coefficients and stable average friction coefficients of the GSEC film coated archwires reach the highest values of 0.29 and 0.19 after 30 days of immersion, respectively, as specifically shown in Fig. 7(c). However, the low friction coefficient of less than 0.20 could be retained even after 30 days of immersion periods.

Optical images of worn surfaces on the GSEC film coated archwires before and after friction tests are given in Figs. 7(d). Small cracks were observed on the surfaces of the GSEC film coated archwires, the number of cracks increases with the extension of immersion periods. The cracks could be considered as the corrosion of the GSEC film during the immersion periods in the artificial saliva solution. Several delaminations of the GSEC film are randomly found on the surfaces of the archwires, including inside and outside of the wear tracks. Continuous tribofilms are accumulated inside of the wear tracks. Besides, mild wear is maintained on the brackets, as evidenced in Fig. S8 in ESM.

3.5 Low friction mechanism of GSEC film coated archwire

Low friction and high wear resistance of the archwire-bracket tribo-pairs are achieved under artificial saliva environment with the production of the carbon films, especially the GSEC films fabricated on the stainless steel archwires. In order to gain more insights into the low friction mechanism, worn surfaces on the carbon film coated archwires were analyzed by the Raman spectroscopy and 3D laser confocal microscopy, as shown in Figs. 8 and 9, respectively.

Raman spectra and derived deconvolution curves of the worn surfaces on the carbon film coated

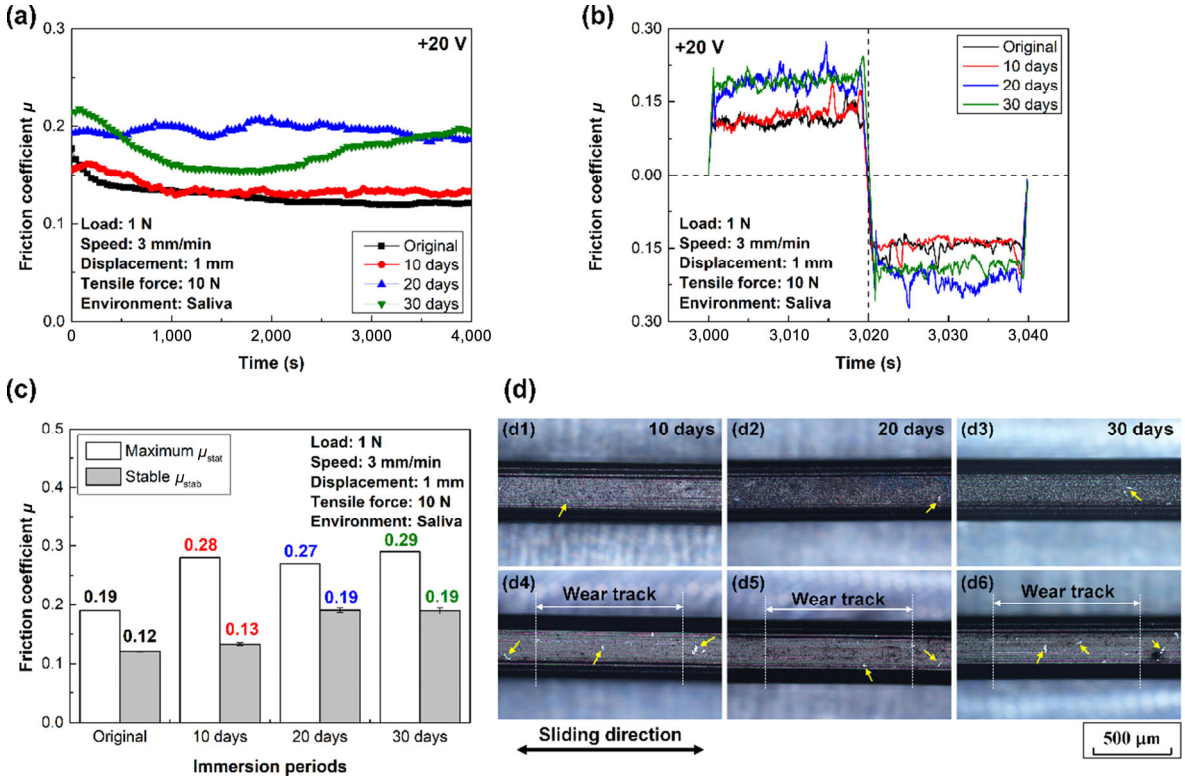

Fig. 7 Friction and wear behaviors of the contact combination of the GSEC film coated archwires and brackets under artificial saliva environment after different immersion periods (0, 10, 20, and 30 days) in artificial saliva solution. The GSEC film was fabricated at substrate bias voltage of +20 V. (a) Mean friction coefficients of each cycle. (b) Typical friction curves in one cycle at steady state from 3,000 to 3,040 s. (c) Maximum static friction coefficients and stable average friction coefficients. (d) Optical images of worn surfaces on the GSEC film coated archwires before and after friction test. Delamination of the GSEC films are denoted by yellow arrows.

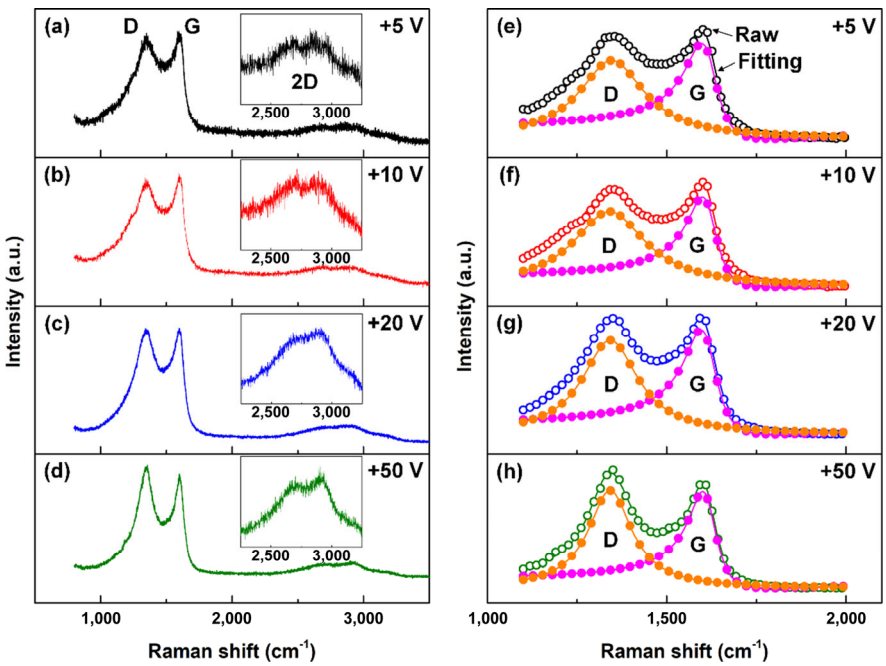

Fig. 8 Raman spectra and corresponding deconvolution curves (a Lorentzian peak for the D band and a BFW peak for the G band) of the worn surfaces on the carbon film coated archwires prepared at substrate bias voltages of (a, e) +5 V, (b, f) +10 V, (c, g) +20 V, and (d, h) +50 V. Enlarged views of the 2D peaks are shown in the inset images.

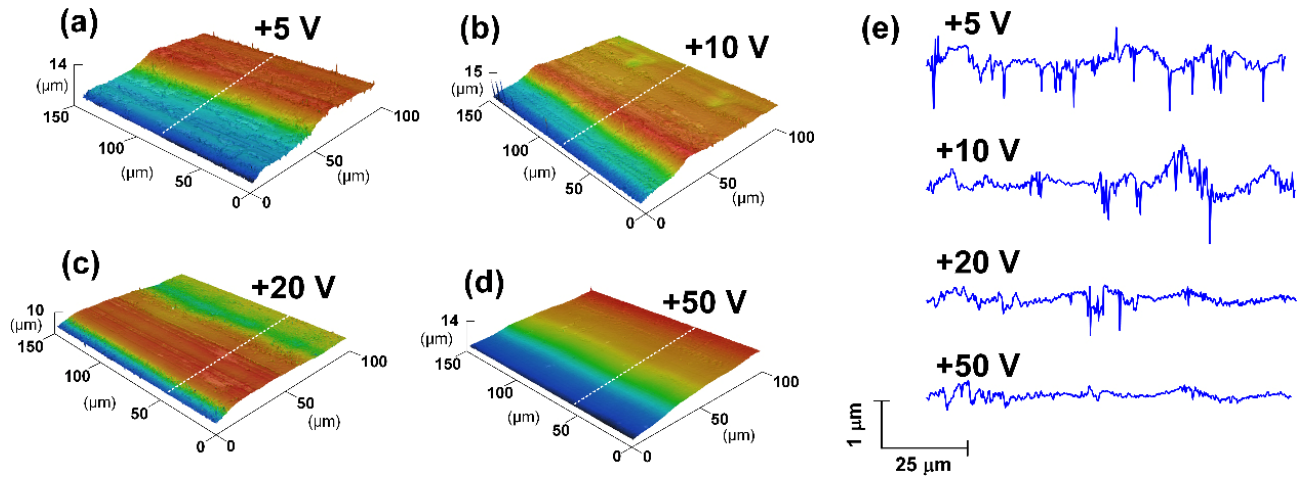

Fig. 9 Surface morphological characteristics of worn surfaces on the carbon film coated archwires. (a–d) 3D optical images and (e) corresponding cross-sectional profiles of the worn surfaces of the carbon film coated archwires after sliding against brackets under artificial saliva environment.

archwires are shown in Fig. 8. Compared with Raman spectra of the as-deposited carbon films in Fig. 3, the appearance of two separate 2D peaks reveals the existence of graphene nanocrystalline structures on the worn surfaces of all four types of carbon films. Therefore, it is suggested that a transformation from nominal amorphous structure to graphene sheets embedded nanostructure inside of the carbon film arises during the sliding friction tests, especially for the carbon films prepared under substrate bias voltages of +5 and +10 V. Moreover, the Raman analysis results, as provided in Table 4, demonstrate higher values of I_D/I_G in relation to those in Table 3. Furthermore, the I_D/I_G increases from 0.82 to 1.01 with increasing substrate bias voltage from +5 to +50 V as well. It is therefore argued that the low friction behavior of the carbon film, particularly the GSEC film, is highly related to the formation of the graphene nanocrystallites in the local structures. Surface morphological characteristics of worn surfaces on the carbon film coated archwires after sliding against brackets under the artificial saliva environment are shown in Fig. 9. Peaks and valleys in the profiles of the carbon film are strongly related to the delamination of the carbon film during the friction test. It is found that smooth surfaces are obtained together with low friction coefficient in carbon film deposited at higher substrate bias voltages.

In summary, the low friction mechanisms of the GSEC film coated archwire sliding against bracket in the artificial saliva environment is proposed and a schematic diagram is shown in Fig. 10. Figure 10(a) demonstrates the initial state of the archwire-bracket contact combination. The low friction performance is mainly attributed to the formation of a tribofilm during the running-in stage (Fig. 10(b)) and a salivary adsorbed film at the steady state (Fig. 10(c)). Firstly, the fabrication of carbon film onto the archwire surface could directly inhibit the metal-metal contact, where the intensive abrasive and adhesive wear of the stainless steel material cause high friction coefficient up to 0.60. Generally, the extraordinary nanostructure of the carbon-based films facilitates the formation of carbon tribofilm to reduce the shear strength of the sliding contacts, thus acting as a solid lubrication layer and leading to the low friction coefficient of less than 0.20 for the archwire-bracket contact system [36, 37]. The existence and/or generation of graphene nanocrystallites in the contact interfaces of amorphous carbon film [34, 44], GSEC film [34, 44] as well as graphene nanocrystallited carbon nitride (GNCN) film

Table 4 Raman analysis results of the worn surfaces on the carbon film coated archwires after friction tests.

Substrate bias voltage (V)	D peak (cm^{-1})	I_D/I_G
+5	1,347	0.82
+10	1,340	0.84
+20	1,342	0.90
+50	1,342	1.01

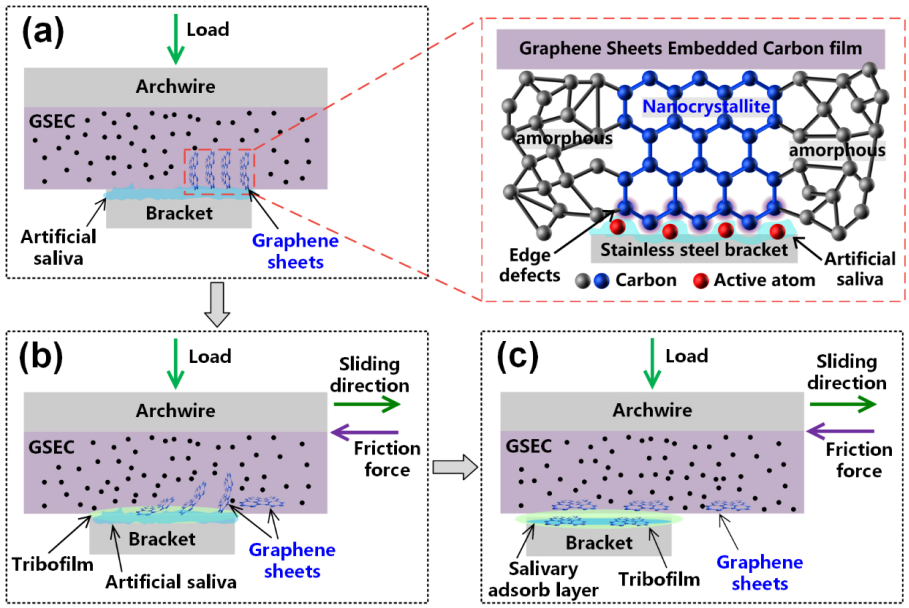

Fig. 10 Low friction mechanism of the GSEC film coated archwire sliding against bracket in artificial saliva environment. (a) Initial state of the archwire-bracket contact combination. Detailed nanostructures of the GSEC films are shown in the inset image. (b) Reduction of friction coefficient during the running-in stage. (c) Stable low friction state of the archwire coated with the GSEC film with the formation of tribofilm containing graphene sheets as well as salivary adsorb layer.

[31, 32] have been clarified to be beneficial for achieving the friction coefficients of lower than 0.10. Thus, the formation of highly ordered graphene nanocrystalline structures together with the graphene edge defects [28–30], which were evidenced from TEM and Raman analyses, undergo the combined effects of compressing and shearing stress, facilitate the emerging of graphene sheets aligned to sliding direction in the tribofilm with extremely low shear force (van der Waals force [49]).

Secondly, the roles of the artificial saliva in the friction and wear performances of the archwire-bracket sliding contacts have been extensively explored in the previous researches [15, 36, 37, 50–53]. On the one hand, the artificial saliva flowing into the contact interfaces is favorable for generating a salivary protein adsorbed layer, the multilayer structures of the adsorbed layer provide low boundary friction coefficient through a complicated interaction between mucins and lower-molecular weight proteins [52, 54]. Hence, a slight decrease of stable friction coefficient from 0.17 to 0.12 is observed in the GSEC film coated archwires under mild wear condition. On the other hand, the insertion of active atoms, such as Cl, from the artificial saliva solution [53] and the following chemical reactions with the amorphous carbon matrix, resulting in the appearance of cracks and delamination of the carbon film on the worn surface of the carbon film coated archwire in some cases, a relatively higher friction coefficient of less than 0.30 are observed for the GSEC film coated archwires after different immersion periods.

Finally, it is concluded that coupling effects of the generation of the salivary adsorbed layer with a continuous supply of the artificial saliva as well as dynamic friction-induced formation and transfer of graphene sheets on the contact interfaces are beneficial for obtaining robust low friction and low wear behaviors of the GSEC film coated archwires, which suggest their potential applications in clinical orthodontic treatments in the near future.

4 Conclusions

In summary, the local microstructures of the carbon films prepared by using the customized MCECR plasma sputtering system evolve from amorphous carbon to graphene nanocrystallites with the increase of the substrate bias voltage from +5 to +50 V. Graphene sheets embedded carbon films are successfully

fabricated under substrate bias voltages of +20 and +50 V. Moreover, low friction coefficients and high wear resistance of the GSEC film coated archwires are achieved when sliding against stainless steel brackets in artificial saliva environments. Furthermore, the low friction behaviors of the GSEC film coated archwires sustain even after 30 days of immersion in artificial saliva solution. The excellent friction and wear performances of the GSEC film coated archwires have been attributed to the formation of salivary adsorbed layer and graphene sheets rich tribofilm on the contact interfaces. With the application of surface coating technique using GSEC film, it is expected that the orthodontic treatment could be more effective and efficient with improved quality of patient care.

Acknowledgements

The authors would like to appreciate the Shenzhen Fundamental Research Project (JCYJ20180305125239722 and JCYJ20160427105015701) and National Natural Science Foundation of China (51405308). Mr. Xiaoyi Luo is also thanked for the preparation of the 3D illustration of the experimental apparatus. The Electron Microscope Center (EMC) of Shenzhen University is kindly appreciated for instrument time and technical support in SEM-EDS and TEM-EELS characterizations.

Electronic Supplementary Material: Supplementary material is available in the online version of this article at https://doi.org/10.1007/s40544-020-0471-3.

References

[1] Feu D, de Oliveira B H, de Oliveira Almeida M A, Kiyak H A, Miguel J A M. Oral health-related quality of life and orthodontic treatment seeking. *American Journal of Orthodontics and Dentofacial Orthopedics* **138**: 152–159 (2010)

[2] Tang W, Tian J, Zheng Q, Yan L, Wang J, Li Z, Wang Z L. Implantable self-powered low-level laser cure system for mouse embryonic osteoblasts' proliferation and differentiation. *ACS Nano* **9**: 7867–7873 (2015)

[3] Benson P E, Javidi H, DiBiase A T. What is the value of orthodontic treatment? *British Dental Journal* **218**: 185–190 (2015)

[4] Liu X, Peng L, Meng J, Zhu Z, Han B, Wang S. Protein-mediated anti-adhesion surface against oral bacteria. *Nanoscale* **10**: 2711–2714 (2018)

[5] Firdanigrum F, Rochadi K, Primasari A. Senior high school students references in choosing orthodontic treatment provider: a study in marelan subdistrict 2018. *Britain International of Humanties and Social Sciences Journal* **2**: 264–270 (2020)

[6] Kusy R P, Whitley J Q, Prewitt M J. Comparison of the frictional coefficients for selected archwire-bracket slot combinations in the dry and wet states. *Angle Orthodontist* **61**: 293–302 (1991)

[7] Kusy R P, Whitley J Q. Resistance to sliding of orthodontic appliances in the dry and wet states: influence of archwire alloy, interbracket distance, and bracket engagement. *Journal of Biomedical Materials Research* **52**: 797–811 (2000)

[8] Thorstenson G A, Kusy R P. Comparison of resistance to sliding between different self-ligating brackets with second-order angulation in the dry and saliva states. *American Journal of Orthodontics and Dentofacial Orthopedics* **121**: 472–482 (2002)

[9] Seo Y J, Lim B S, Park Y G, Yang I H, Ahn S J, Kim T W, Baek S H. Effect of tooth displacement and vibration on frictional force and stick-slip phenomenon in conventional brackets: a preliminary in vitro mechanical analysis. *European Journal of Orthodontics* **37**: 158–163 (2015)

[10] Burrow S J. Friction and resistance to sliding in orthodontics: a critical review. *American Journal of Orthodontics and Dentofacial Orthopedics* **135**: 442–447 (2009)

[11] Tageldin H, Cadenas de Llano Perula M, Thevissen P, Celis J P, Willems G. Resistance to sliding in orthodontics: a systematic review. *Jacobs Journal of Dentistry and Research* **3**: 1–32 (2016)

[12] Savoldi F, Papoutsi A, Dianiskova S, Dalessandri D, Bonetti S, Tsoi J K H, Matinlinna J P, Paganelli C. Resistance to sliding in orthodontics: misconception or method error? a systematic review and a proposal of a test protocol. *Korean Journal of Orthodontics* **48**: 268–280 (2018)

[13] Katz A, Redlich M, Rapoport L, Wagner H D, Tenne R. Self-lubricating coatings containing fullerene-like WS_2 nanoparticles for orthodontic wires and other possible medical applications. *Tribology Letters* **21**: 135–139 (2006)

[14] Akaike S, Kobayashi D, Aono Y, Hiratsuka M, Hirata A, Hayakawa T, Nakamura Y. Relationship between static friction and surface wettability of orthodontic brackets coated with diamond-like carbon (DLC), fluorine-or silicone-doped DLC coatings. *Diamond and Related Materials* **61**: 109–114 (2016)

[15] Wei S, Shao T, Ding P. Improvement of orthodontic friction by coating archwire with carbon nitride film. *Applied Surface Science* **257**: 10333–10337 (2011)

[16] Muguruma T, Iijima M, Brantley W A, Mizoguchi I. Effects of a diamond-like carbon coating on the frictional properties of orthodontic wires. *Angle Orthodontist* **81**: 141–148 (2011)

[17] Zhang H, Guo S, Wang D, Zhou T, Wang L, Ma J. Effects of nanostructured, diamondlike, carbon coating and nitrocarburizing on the frictional properties and biocompatibility of orthodontic stainless steel wires. *Angle Orthodontist* **86**: 782–788 (2016)

[18] Bącela J, Łabowska M, Detyna J, Zięty A, Michalak I. Functional coatings for orthodontic archwires—A review. *Materials* **13**: 3257 (2020)

[19] Novoselov K S, Geim A K, Morozov S V, Jiang D, Zhang Y, Dubonos S V, Grigorieva I V, Firsov A A. Electric field effect in atomically thin carbon films. *Science* **306**: 666–669 (2004)

[20] Hu W, Peng C, Luo W, Lv M, Li X, Li D, Huang Q, Fan C. Graphene-based antibacterial paper. *ACS Nano* **4**: 4317–4323 (2010)

[21] Chung C, Kim Y K, Shin D, Ryoo S R, Hong B H, Min D H. Biomedical applications of graphene and graphene oxide. *Accounts of Chemical Research* **46**: 2211–2224 (2013)

[22] Jia Z, Shi Y, Xiong P, Zhou W, Cheng Y, Zheng Y, Xi T, Wei S. From solution to biointerface: graphene self-assemblies of varying lateral sizes and surface properties for biofilm control and osteodifferentiation. *ACS Applied Materials and Interfaces* **8**: 17151–17165 (2016)

[23] Lu N, Wang L, Lv M, Tang Z, Fan C. Graphene-based nanomaterials in biosystems. *Nano Research* **12**: 247–264 (2019)

[24] Kawai S, Benassi A, Gnecco E, Söde H, Pawlak R, Feng X, Müllen K, Passerone D, Pignedoli C A, Ruffieux P, Fasel R, Meyer E. Superlubricity of graphene nanoribbons on gold surfaces. *Science* **351**: 957–961 (2016)

[25] Berman D, Erdemir A, Sumant A V. Approaches for achieving superlubricity in two-dimensional materials. *ACS Nano* **12**: 2122–2137 (2018)

[26] Hod O, Meyer E, Zheng Q, Urbakh M. Structural superlubricity and ultralow friction across the length scales. *Nature* **563**: 485–492 (2018)

[27] Chen X, Li J. Superlubricity of carbon nanostructures. *Carbon* **158**: 1–23 (2020)

[28] Wang C, Diao D F. Self-magnetism induced large positive magnetoresistance at room temperature region in graphene nanocrystallited carbon film. *Carbon* **112**: 162–168 (2017)

[29] Huang L L, Cao Y Y, Diao D F. Nanosized graphene sheets induced high electrochemical activity in pure carbon film. *Electrochimica Acta* **262**: 173–181 (2018)

[30] Zhang X, Lin Z Z, Peng D, Ye L, Zang J F, Diao D F. Edge-state-enhanced ultrahigh photoresponsivity of graphene nanosheet-embedded carbon film/silicon heterojunction. *Advanced Materials Interfaces* **6**: 1802062 (2019)

[31] Wang P, Zhang W Q, Diao D F. Low friction of graphene nanocrystallite embedded carbon nitride coatings prepared with MCECR plasma sputtering. *Surface and Coatings Technology* **332**: 153–160 (2017)

[32] Wang P, Xue P, Chen C, Diao D F. Structural and tribological behaviors of graphene nanocrystallited carbon nitride films. *Applied Surface Science* **495**: 143591 (2019)

[33] Diao D F, Wang C, Fan X. Frictional behavior of nanostructured carbon films. *Friction* **1**(1): 63–71 (2013)

[34] Sun K, Diao D F. Current density effect on current-carrying friction of amorphous carbon film. *Carbon* **157**: 113–119 (2020)

[35] Huang L L, Cao Y Y, Diao D F. Electrochemical activation of graphene sheets embedded carbon films for high sensitivity simultaneous determination of hydroquinone, catechol and resorcinol. *Sensors and Actuators B: Chemical* **305**: 127495 (2020)

[36] Huang S Y, Huang J J, Kang T, Diao D F, Duan Y Z. Coating NiTi archwires with diamond-like carbon films: reducing fluoride-induced corrosion and improving frictional properties. *Journal of Materials Science-Materials in Medicine* **24**: 2287–2292 (2013)

[37] Kang T, Huang S Y, Huang J J, Li Q H, Diao D F, Duan Y Z. The effects of diamond-like carbon films on fretting wear behavior of orthodontic archwire-bracket contacts. *Journal of Nanoscience and Nanotechnology* **15**: 4641–4647 (2015)

[38] Zhang M, Liu X, Shang H, Lin J. Comparison of TiN and CN_x coatings on orthodontic stainless steel: tribological and biological evaluation. *Surface and Coatings Technology* **362**: 381–387 (2019)

[39] Wang C, Zhang X, Diao D. Nanosized graphene crystallite

induced strong magnetism in pure carbon films. *Nanoscale* **7**: 4475–4481 (2015)

[40] Wang C, Diao D, Fan X, Chen C. Graphene sheets embedded carbon film prepared by electron irradiation in electron cyclotron resonance plasma. *Applied Physics Letters* **100**: 231909 (2012)

[41] Chen C, Fan X, Diao D F. Low-energy electron irradiation induced top-surface nanocrystallization of amorphous carbon film. *Applied Surface Science* **384**: 341–347 (2016)

[42] Zhang W Q, Diao D F, Sun K, Fan X, Wang P. Study on friction-electrification coupling in sliding-mode triboelectric nanogenerator. *Nano Energy* **48**: 456–463 (2018)

[43] Xue P, Chen C, Diao D F. Ultra-sensitive flexible strain sensor based on graphene nanocrystallite carbon film with wrinkle structure. *Carbon* **147**: 227–235 (2019)

[44] Sun K, Fan X, Zhang W Q, Xue P, Diao D F. Contact-focusing electron flow induced nanosized graphene sheets formation in amorphous carbon film for fast low-friction. *Carbon* **149**: 45–54 (2019)

[45] Sánchez-López J C, Erdemir A, Donnet C, Rojas T C. Friction-induced structural transformations of diamondlike carbon coatings under various atmospheres. *Surface and Coatings Technology* **163–164**: 444–450 (2003)

[46] Fan X, Diao D F. Ion excitation and etching effects on top-surface properties of sp^2 nanocrystallited carbon films. *Applied Surface Science* **462**: 669–677 (2018)

[47] Guo M, Diao D, Yang L, Fan X. Restructured graphene sheets embedded carbon film by oxygen plasma etching and its tribological properties. *Applied Surface Science* **357**: 771–776 (2015)

[48] Barbosa L M, da Silva Jr W M, de Mello J D B. Orthomicrotribometer. *Wear* **426–427**: 1729–1739 (2019)

[49] Wang G, Dai Z, Wang Y, Tan P, Liu L, Xu Z, Wei Y, Huang R, Zhang Z. Measuring interlayer shear stress in bilayer graphene. *Physical Review Letters* **119**: 036101 (2017)

[50] Thorstenson G A, Kusy R P. Resistance to sliding of self-ligating brackets versus conventional stainless steel twin brackets with second-order angulation in the dry and wet (saliva) states. *American Journal of Orthodontics and Dentofacial Orthopedics* **120**: 361–370 (2001)

[51] Bongaerts J H H, Rossetti D, Stokes J R. The lubricating properties of human whole saliva. *Tribology Letters* **27**: 277–287 (2007)

[52] Dridi A, Bensalah W, Mezlini S, Tobji S, Zidi M. Influence of bio-lubricants on the orthodontic friction. *Journal of the Mechanical Behavior of Biomedical Materials* **60**: 1–7 (2016)

[53] Nanjundan K, Vimala G. Evaluation of frictional resistance and surface characteristics after immersion of orthodontic brackets and wire in different chemical solutions: a comparative *in vitro* study. *Indian Journal of Dental Research* **27**: 513–520 (2016)

[54] Yakubov G, Macakova L, Wilson S, Windust J, Stokes J. Aqueous lubrication by fractionated salivary proteins: synergistic interaction of mucin polymer brush with low molecular weight macromolecules. *Tribology International* **89**: 34−45 (2015)

Zonglin PAN. He received his bachelor degree from Central South University of Forestry and Technology, Changsha, China, in 2017. Then he was a graduate student in Institute of Nanosurface Science and Engineering (INSE) at Shenzhen University, Shenzhen, China. His research interests include the low friction mechanisms of solid lubrication coatings in oral tribology.

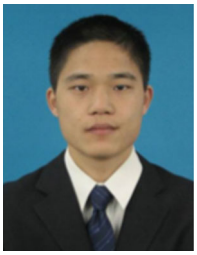

Pengfei WANG. He obtained his B.S. and M.S. degrees from Xi'an Jiaotong University, Xi'an, China, in 2004 and 2007, respectively, and the Ph.D. degree from Tohoku University, Sendai, Japan, 2011. He currently is an associate researcher for Institute of Nanosurface Science and Engineering (INSE) at Shenzhen University, Shenzhen, China. His current researches are focused on the super-low friction and tribo-electrification of micro and nano surfaces.

Dongfeng DIAO. He obtained his Ph.D. degree in mechanical engineering from Tohoku University, Sendai, Japan, 1992. He currently is a distinguished professor and director for Institute of Nanosurface Science and Engineering (INSE) and Electron Microscope Center (EMC) at Shenzhen University, Shenzhen, China. He is a foreign member of the Engineering Academy of Japan (EAJ). His research interests include nanosurface science and technology, nanotriboelectronics, quantum tribology, and contact-electrification based sensor technology.